The published version is at Fuel 102:613–623, 2012, http://doi.org/10.1016/j.fuel.2012.06.107

Spray characterization of gasoline-ethanol blends from a multi-hole port fuel injector

Anand T.N.C.[a,*], MadanMohan A.[b] and Ravikrishna R.V.[b]

[a] Department of Mechanical Engineering, Indian Institute of Technology Madras, Chennai - 600036, India.

[b] Department of Mechanical Engineering, Indian Institute of Science, Bangalore – 560012, India.

Abstract

This work reports the measured spray structure and droplet size distributions of ethanol-gasoline blends for a low-pressure, multi-hole, port fuel injector (PFI). This study presents previously unavailable data for this class of injectors which are widely used in automotive applications. Specifically, gasoline, ethanol, and gasoline-ethanol blends containing 10%, 20% and 50% ethanol were studied using laser backlight imaging, and particle/droplet image analysis (PDIA) techniques. The fuel mass injected, spray structure and tip penetrations, droplet size distributions, and Sauter mean diameter were determined for the blends, at two different injection pressures. Results indicate that the gasoline and ethanol sprays have similar characteristics in terms of spray progression and droplet sizes in spite of the large difference in viscosity. It appears that the complex mode of atomization utilized in these injectors involving interaction of multiple fuel jets is fairly insensitive to the fuel viscosity over a range of values. This result has interesting ramifications for existing gasoline fuel systems which need to handle blends and even pure ethanol, which is one of the renewable fuels of the future.

Keywords: Port Fuel Injector, spray characterization, PDIA, gasoline-ethanol blends

* Corresponding author. Email: anand@iitm.ac.in, Tel: +91(44)22574715, Fax: +91(44)2257 4652

1. Introduction

Depleting petroleum resources, increasing costs, and requirements of energy security, have led to an increase in the interest in renewable bio-fuels, especially in recent years. One such bio-fuel which has seen wide use as blends with conventional fuels is ethanol. Countries such as Brazil, the U.S.A, and India have mandated blending of ethanol with gasoline or diesel in various proportions. Hence, there are studies in the literature on engine-related studies of gasoline-ethanol blends comparing the power output and average emissions (1–3). While such studies give an overall picture which is useful, it is more illuminating to study the differences in engine processes which occur due to the differences in fuel, as these studies could bring out the scope for potential improvement and optimization of a process based on the fuel. The processes which are expected to be affected by fuel composition include fuel injection and atomization, evaporation, and combustion. The only studies which deal with such processes for gasoline-ethanol blends have focused on gasoline direct injection (GDI) (4,5). The spray structure from GDI injectors is completely different from that of port fuel injection (PFI) injectors since the injection pressures and the nozzle geometries are very different. GDI injection pressures are in the range of a few MPa, and typically involve hollow cone sprays. PFI systems, on the other hand, involve very low pressures (0.2 – 0.6 MPa), and involve plate type injectors. Additionally, with PFI systems, there is a challenge of achieving satisfactory atomization, since the injection pressures are very low. This was one of the motivations of our study.

The vast majority of automotive systems, both four-wheelers and two-wheelers, use port fuel injectors. The atomization process in these low-pressure sprays is extremely complex, and involves formation of multiple liquid jets,

interaction of these near-parallel but closely-spaced jets, and the consequent breakup into ligaments and droplets. There is no study to date in the literature pertaining to spray structure and droplet sizing of blends of gasoline-ethanol from these multi-hole port fuel injectors, and the present work addresses this gap in the literature. In the following sections, the experimental setup, techniques and the methodology followed in the experiments are briefly described, followed by a discussion of experiment results.

2. Experimental Setup

The experimental setup used for the study is briefly described here, and has been explained in more detail in an earlier work (6). It consists of a low-pressure 4-hole gasoline injector (Figure 1), typical of injectors used currently in port fuel injection engines. The fuel is pressurized by means of compressed nitrogen, and transducers measure the fuel temperature and the fuel line pressure close to the injector. The injector is actuated by means of an electronic circuit, and the timing of the injection pulse and the pulse duration are controlled by means of a computer with a LaVision programmable timing unit. A schematic of the setup used is shown in Figure 2. The fuel was sprayed into the ambient (pressure of 0.9 bar and temperature 25°C). The spray from the injector was characterized by optical techniques, as described in the following section.

3. Methodology

Particle/droplet image analysis (PDIA) is an image-based technique in which digital images of small regions of the spray are analyzed using particle detection algorithms. Kashdan et al. (7,8) compared PDIA results with those obtained from Phase Doppler Anemometry (PDA). Their experiments with a spray having most

of the droplets in the range of 5 µm to 30 µm showed that PDIA compares very well with PDA. They also observed that the PDIA technique has the advantage of being able to size large droplets which are typically not truly spherical, and hence would be rejected or incorrectly sized by PDA. Another advantage of PDIA over PDA is the ability to measure droplets over a much larger size range. These advantages make PDIA more suitable for low pressure sprays such as PFI sprays, which consist of a large range of droplets, as well as non-spherical droplets.

In the present study, backlit images of the spray exiting the injector were acquired using a 14 bit CCD camera (2048 x 2048 pixels). Illumination for the images was provided by a pulsed Nd:YAG laser utilized in conjunction with a diffuser containing fluorescent plates for uniform backlighting. Images were taken using a Nikon 105 mm lens when the entire spray was required to be visualized - to compare spray structures or spray tip penetrations. In order to measure droplet sizes, a much smaller region of the spray (4.8 mm x 4.8 mm) was photographed using a long distance QM1 Microscope. Droplet sizing was conducted at a location 100 mm from the injector tip along the axis with the injection duration maintained as 5 ms, as recommended by the SAE standard for PFI systems titled "Gasoline Fuel Injector Spray Measurement and Characterization – A New SAE J2715 Recommended Practice", 2008 (9). Images of the spray were taken at different times after the start of injection, and processed using the DaVis software. In order to obtain statistically significant results, images of 400 successive spray events were taken at each setting. The procedure was repeated for different fuels – 100% gasoline, 100% ethanol, and mixtures of gasoline and ethanol containing 10%, 20%, or 50% ethanol by volume, at injection pressures of 0.25 MPa and 0.6 MPa.

4. Results and Discussion

Figure 3 shows instantaneous images of the spray with pure gasoline, and pure ethanol as fuel at an injection pressure of 0.25 MPa. It is observed that in both cases, a liquid core is present near the nozzle with large ligaments forming, which further break up into droplets far away from the injector. From the magnified images, it is observed that close to the injector, the ethanol spray appears to have larger and thinner, sheet-like ligaments. At the injection pressures studied, it is observed that the sprays from the four jets interact. It is also observed that as the pressure increases, the velocity increases which in turn causes higher inertial forces. This in turn will lead to faster growth of instabilities which in turn will lead to increased interaction between the jets. It is believed that the sheet-like ligaments are formed close to the injector due to the interaction between the jets.

The effect of the interaction between the jets (or the effect of the absence of such an interaction) is clearly understood from Figure 4, which shows gasoline and ethanol sprays from a single hole PFI injector. It is observed that the single jet does not breakup at all even upto 30 mm from the injector, whereas the spray from the 4-hole injector breaks up within 10 mm of the injector due to the interaction between the multiple jets. Thus, it is seen that the mechanism of spray breakup in PFI injectors is fundamentally different from that in GDI injectors where conventional breakup of single jets occur due to high pressure injection.

Gasoline and ethanol have similar surface tension values. The viscosity of ethanol is, however, higher. The structures (in Figure 3) are more prominent in the case of ethanol due to the higher viscosity which reduces the tendency of the ligaments to break up. However, in both cases, the ligaments breakup as we move away from the injector, and on a macroscopic scale, no significant differences are observed between the ethanol and gasoline spray structure.

When instantaneous images of the sprays are ensemble averaged, average images of the progression of the spray are obtained, as shown for gasoline in Figure 5. It was concluded from the ensemble-averaged images that the spray starts leaving the injector at around 1.4 ms after the transmission of the electronic pulse for both ethanol and gasoline, i.e., the lag between the electronic and hydraulic injection times appears to be the same for both the fuels. The extent of travel of the spray is also not very different. This is seen clearly in Figure 6 which shows the spray tip penetrations which were obtained by processing the ensemble-averaged images, at injection pressures of 0.25 MPa and 0.6 MPa, for pure ethanol, pure gasoline and 50% ethanol-gasoline blend. The tip penetrations were obtained from the ensemble averaged images by inverting the averaged image and subtracting the inverted background. The images were then converted to a binary format after applying a threshold. The same procedure was followed for all the cases.

In Figure 6, as expected, the tip penetrations are larger for the 0.6 MPa case than for the 0.25 MPa case, at any point of time. However, for a given pressure, in the time duration investigated, the spray tip penetrations are observed to be nearly identical for all three fuels. This trend is similar to that found in literature for high pressure GDI sprays (5) of gasoline-ethanol blends.

At the injection pressure of 0.25 MPa, the variation of spray tip penetration with time for gasoline has been fitted to

$$y = -0.07257t^3 - 1.229t^2 + 30.26t - 36.47 \qquad \text{Eq. (1)}$$

with the goodness of fit given by an R^2 value of 0.999 and root mean square error of 0.425. In this expression, the time t is in milli seconds (t>1.4 ms to take into account the delay between the electronic and hydraulic time), and the tip penetration is in mm. At the injection pressure of 0.6 MPa, the variation of spray tip penetration with time for gasoline has been fitted to

$$y = -6.037t^3 + 2.1359t^2 + 30.1t - 40.76 \quad \text{Eq. (2)}$$

with the goodness of fit given by an R^2 value of 0.997 and root mean square error of 1.78.

Estimates of the mass injected per injection pulse were obtained by collecting the fuel injected for 200 sprays and measuring it with a mass balance. Statistical independence of the results was verified by considering 200 and 300 cycles as the measurement duration. The accuracy of the mass balance utilized is 1 mg and a typical measurement of fuel quantity for 200 cycles is around 1750 mg, with a precision of ±10 mg. This gives a comprehensive error bar (considering both accuracy and precision) of 0.6%.

The measured values of mass injected for gasoline, ethanol and 50% ethanol blend, are shown in Table 1. It is observed that the values of mass injected are higher for ethanol. When considered on a volume basis, however, the values differ by less than 10% (It should be noted here that a value of density of 734 kg/m^3 was measured for gasoline, and the density of ethanol is 789 kg/m^3 as noted in Table 2). Hence, the volume flow rates being similar, similar velocities are expected, which explains the similar spray tip penetration curves for these fuels.

The spray cone angle is estimated from the images using an algorithm developed by Gandhi and Meinhart (10). The algorithm computes the left and right spray boundaries from the nozzle tip starting with an angle of 1° with an increment of 0.5°. It computes the spray area included between the lines and finds the cone angle when the spray area between the lines is above 90%. Figure 7 shows the increase in the cone angle with increase in injection pressure. It is observed that the ethanol spray has a slightly higher cone angle compared to gasoline and the gasoline-ethanol blend. This might be due to the higher interaction between the

ethanol jets as was observed in Figure 3, and the slightly higher quantity of the ethanol injected compared to the other cases.

Figure 8 shows a sample microscopic image of the spray at 100 mm from the injector tip along the axis, where the fuel droplets are visible. The image shows droplets which are in the focal plane as well as droplets which are out of focus and hence appear blurred. The blurred droplets are not in the region of interest, and are hence ignored. The image also highlights the droplets identified by the PDIA technique, and indicates their diameters. Droplet sizes shown here were estimated using the LaVision Particle Master Shadow module. Images are first inverted and corrected for the background. All parts of the inverted image that are above a global threshold (value used = 25 % of maximum intensity) are segmented, so that each segment consists of contiguous pixel areas. Regions of the image which have an intensity less than the global threshold are ignored. For each segment, two different particle areas are calculated: One area using the Low level threshold (value used = 35 % of the maximum intensity) and another area using the High level threshold (value used = 65 % of the maximum intensity). The low level diameter is much higher than the high level diameter for diffuse, out of focus particles. To exclude defocused particles from the analysis, only particles which have a low level diameter less than 150 % of the high level diameter are considered. The values of all the criteria used above were arrived at by processing images of the mono-disperse spray and focused and defocused images of a standard calibration plate. Droplets appear sharp if they are near the focal plane of the long distance microscope. Droplets which are far away from the focal plane are outside the field of interest and appear blurred and larger than their focused size. Such droplets are not sized. Figure 9 shows images of the calibration plate at

different distances from the focal plane. The blurring of the patterns on the target can be observed as the plate is moved away from focal plane.

Depth of focus correction was also performed within the software. In the present study, each pixel of the images acquired corresponds to 2.4 µm, and hence droplets of size 10 µm or less have not been considered. In order to obtain statistically significant values, the results from 400 images were obtained corresponding to each point of time, for each fuel and pressure. These results are statistically independent of the number of images, with the maximum variation in the SMD being less than 3% when the number of images is changed from 400 to 500.

The accuracy of the technique and the processing was evaluated by performing droplet sizing measurements on a stream of mono-disperse droplets created by a mono-disperse droplet generator (Artium Technologies Inc.: MDG 100). Figure 10 shows the distribution obtained for 726 particles. The pre-set value of the Sauter mean diameter (SMD) in the droplet generator was 135 µm. Using the PDIA technique, the value of SMD obtained was 136.8 µm with an arithmetic mean diameter of 136.7 µm. Thus, the accuracy of the technique in measuring the SMD can be observed to be within 1% for the mono-disperse droplets studied. For the spray, the accuracy is estimated to be $< \pm 5\%$ (which is the cumulative error considering precision, accuracy and repeatability).

Figure 11 and Figure 12 show the variation of Sauter mean diameter (SMD) with time for the different blends, at injection pressures of 0.25 MPa, and 0.6 MPa, respectively. It is observed that the SMDs are initially high as large droplets enter the measurement volume before the small droplets, since they retain a higher portion of the initial momentum. The SMD then remains fairly constant–

this corresponds to the steady part of the spray where the mass flow rate, and hence the SMD remain constant, following which, the SMDs reduce at the last point, indicating that the injection process has completed, leaving only fine droplets which drift slowly into the region where dropsizing is conducted. The SMD values in the steady part of the spray vary from around 110 micron at an injection pressure of 0.25 MPa, to around 80 micron at an injection pressure of 0.6 MPa, indicating that the higher injection pressure leads to a finer spray, as expected - the SMD has been observed to decrease with increasing injection pressure for GDI, diesel and other types of injectors (11,12). It is interesting to note that at each pressure, the SMDs of the sprays of the different blends do not reveal significant differences. The surface tension values of gasoline and ethanol are 20.8 mN/m and 22.3 mN/m, while their viscosities are in the range of 0.37-0.44 mPa·s and 1.19 mPa·s, respectively (2,13). Thus, though the surface tension values are similar, the viscosity values are considerably different, and hence the atomization and thus the SMDs are expected to be different (14,15). Such a trend is, however, not observed here. The current spray is from a 4-hole low-pressure injector. It is possible that for the present mode of atomization, the breakup mechanism is not sensitive to the range of viscosity encountered in the present study. In other words, the proximity of the four jets from the four nozzle orifices, the interaction of the jets, and the resulting breakup play a much larger role than viscosity. This could offer interesting applications for atomization of high viscosity liquids using such atomizers. The interaction between the jets is clearly visible from Figure 13 which shows images of the close up of the spray. Figure 13 (a), (b) and (c) show gasoline sprays at injection pressures of 0.08 MPa, 0.25 MPa and 0.6 MPa, respectively. It is observed that at an injection pressure of 0.08 MPa, the jets emerge separately, and there is not much of interaction between the jets.

At a higher injection pressure of 0.25 MPa, the jets clearly interact as seen from Figure 13 (b). The interaction between the jets further increases as the injection pressure is increased to 0.6 MPa, as seen from Figure 13 (c).

Droplet distributions at various instants of time (Figure 14 and Figure 15) show interesting trends, with a tendency towards the presence of two peaks corresponding to the time where the droplets first enter the domain under study (Figure 14a and Figure 15a). At later times (Figure 14b and Figure 15b), it is observed that the droplet size distributions are either unimodal or bimodal. Though the number of small droplets is large under all conditions, their contribution to the total volume, and hence the SMD, is small. The arithmetic mean diameter (D10) reduces by around 30 µm between the first image and the second image at each pressure (Figure 14a and Figure 14b at 0.25 MPa, Figure 15a and Figure 15b at 0.6 MPa) indicating that the spray consists of a higher percentage of relatively smaller droplets at later times. However, the SMD (D32) does not show as large a reduction (as seen from the first two points of Figure 11 and Figure 12) since the SMD is influenced more by larger droplets than by small droplets.

Figure 16 and Figure 17 show the SMD at an axial location 50 mm from the injector tip, for injection pressures of 0.25 MPa and 0.6 MPa, respectively. The trends here are similar to those observed earlier from Figure 11 and Figure 12 which corresponded to an axial location of 100 mm, though the first point corresponding to the start of injection is not captured here. The values of SMD at 50 mm are higher than those at 100 mm, indicating that breakup is not complete at this point.

Figure 18 shows a scatter plot of centricity of droplets for pure ethanol at 10 ms after start of injection (SOI) for an injection pressure of 0.25 MPa, at a location 100 mm downstream of the injector. The centricity is defined as the ratio of the minor to the major axis of the droplet - droplets which are perfectly circular in the images have a centricity of 1. A limitation of the imaging technique is that due to the discrete nature of pixels and the small number of pixels forming small droplets, the centricity values for some small droplets (less than 50-100 µm) may be calculated as less than the actual values depending upon the magnification. This is however not a problem with large droplets where the number of pixels forming a droplet are sufficiently large, and hence for these droplets, the centricity values are very reliable. It is observed from Figure 18 that droplets in the range of 100 µm are nearly spherical while there are some droplets larger than 200 µm or so which have low centricity values, indicating that they are not circular. In contrast to these results, as we move closer to the injector, at 50 mm from the injector, we see from Figure 19 that there are a very large number of large droplets which are non-spherical. These are droplets which would potentially be missed or be incorrectly sized using conventional techniques such as PDPA which assume spherical droplets. The effect of ignoring non-spherical droplets is evident from Figure 20, which compares the SMD obtained from considering all droplets, and only droplets which have a centricity of 0.7 or higher, for an injection pressure of 0.25 MPa. It is observed that at a location 100 mm from the injector, most droplets are spherical, and hence the effect is not significant. However, at a location 50 mm from the injector, many large droplets are non-spherical, and if droplets with a centricity lower than 0.7 are ignored, the error in the SMD due to this could be as high as 20%. This indicates that if any technique which ignores very non-spherical droplets (such as PDPA) is used as the droplet sizing technique

for such low pressure sprays, the location of measurement needs to be chosen sufficiently far away from the injector for the SMD to be representative of all the droplets present. In a recent study using the same technique, but at much higher pressures (>600 bar), atomization of highly viscous liquids were studied and the presence of non-spherical droplets was observed (16). However, for less viscous liquids at high pressures, the droplets are likely to be spherical even close to the injector and hence the effect may not be as pronounced.

Figure 21 and Figure 22 show scatter plots of velocity as a function of diameter for an injection pressure of 0.25 MPa, at 50 mm and 100 mm from the injector tip, respectively. The velocity values were obtained by performing particle tracking velocimetry in conjunction with PDIA on images taken using a double pulsed Nd:YAG laser and double frame CCD camera. It is observed that at 50 mm from the injector, large droplets have a maximum velocity of around 22 m/s while the smaller droplets have velocities as low as 5 m/s. At a later time, at a distance of 100 mm from the injector (Figure 22), it is observed that the maximum velocity has dropped to 15 m/s with most droplets having much smaller velocities. Figure 23 shows a similar velocity plot at 100 mm from the injector, at an injection pressure of 0.6 bar. It is observed here that the maximum velocities of the large droplets are higher at around 25 m/s while the bulk of the smaller droplets have velocities in the range of 10 m/s.

The variation of Weber number of the droplets with diameter is shown in Figure 24 and Figure 25 for the ethanol spray, for an injection pressure of 0.25 MPa. These figures correspond to measurement timings of 5 ms and 10 ms, respectively after the start of injection, for respective axial locations of 50 mm and 100 mm.

The Weber number, is defined as the ratio of the aerodynamic force (disruptive force) to the surface tension force (restoring force), and is considered one of the most important parameters when describing secondary atomization (17). It is observed that the Weber number falls in a narrow band for each diameter, reflecting that most droplets of a given diameter have a similar value of velocity. In the present study, it is observed from the figures that the Weber number is below 10 for most of the droplets. According to Guildenbecher et al. (17), for droplets with a Weber number below a value of around 11, the predominant secondary breakup mechanism is vibrational breakup which produces only a few fragments whose sizes are comparable to that of the parent droplet. At 50 mm from the injector, the ethanol spray has an SMD of around 140 µm at 5 ms after the start of injection, which reduces to around 110 µm at 100 mm along the axis at 10 ms after the start of injection. Estimations using the D^2 law indicate a decrease in a diameter of only around 1 µm for a 140 µm droplet. Thus the change of around 30 µm observed indicates that secondary break up (vibrational break up of the droplets) results in a lower SMD between the 50 mm and 100 mm axial locations. At the 100 mm location (Figure 25), however, droplet Weber numbers are below the critical value of 6, and further secondary breakup may not be happening downstream (18).

5. Conclusions

The spray structure, droplet size and velocity measurements for various gasoline-ethanol blends from a 4-hole port fuel injector have been reported. Specifically, the spray structure and the planar drop size measurements were

performed using laser-backlit imaging and PDIA technique at injection pressures of 0.25 MPa and 0.6 MPa. Data has been generated for gasoline, ethanol, and gasoline-ethanol blends containing 10%, 20% and 50% ethanol. The volume of fuel injected at each pressure, and hence the spray penetration, were found to be similar across blends at each injection pressure. Despite a considerable difference in the viscosity of the fuels injected, the droplet sizes were also found to be similar. This is contrary to the expected trend of higher drop sizes with increasing viscosity for a relatively constant surface tension value. It is believed that the design of the injector wherein four streams of liquid emerge from the nozzle almost parallel to the axis, and interact with each other resulting in a unique mode of breakup could be the main reason for the effect of viscosity not being strongly manifested. This observation has interesting ramifications for the utilization of this mode of atomization for other high viscosity fuels in low pressure injection applications.

References

1. Bayraktar H. Experimental and theoretical investigation of usinggasoline–ethanol blends in spark-ignition engines. Renewable Energy. 2005;30:1733–47.

2. Yüksel F, Yüksel B. The use of ethanol-gasoline blend as a fuel in an SI engine. Renewable Energy. 2004;29(7):1181–91.

3. Costa RC, Sodre JR. Hydrous ethanol vs. gasoline-ethanol blend: Engine performance and emissions. Fuel. 2010;89:287–93.

4. Matsumoto A, Moore WR, Lai MC, Zheng Y, Foster M, Xie XB, et al. Spray Characterization of Ethanol Gasoline Blends and Comparison to a

CFD Model for a Gasoline Direct Injector. SAE International Journal of Engines. 2010;3(1):402.

5. Gao J, Jiang D, Huang Z. Spray properties of alternative fuels: A comparative analysis of ethanol-gasoline blends and gasoline. Fuel. 2007;86(10-11):1645–50.

6. Anand TNC, Madan Mohan A, Deshmukh D, Ravikrishna RV. Optical characterization of PFI gasoline sprays: Effect of Injection Pressure. SAE Paper 2010-32-0067. 2010;

7. Kashdan JT, Shrimpton JS, Whybrew A. Two-Phase Flow Characterization by Automated Digital Image Analysis. Part 1: Fundamental Principles and Calibration of the Technique. Particle & Particle Systems Characterization. 2003;20(6):387–97.

8. Kashdan JT, Shrimpton JS, Whybrew A. Two-Phase Flow Characterization by Automated Digital Image Analysis. Part 2: Application of PDIA for Sizing Sprays. Particle & Particle Systems Characterization. 2004;21(1):15–23.

9. Hung DL., Harrington DL, Gandhi AH, Markle LE, Parrish SE, Shakal JS, et al. Gasoline Fuel Injector Spray Measurement and Characterization – A New SAE J2715 Recommended Practice. SAE Paper 2008-01-1068. 2008;

10. Gandhi AH, Meinhart, M.A. . A comparison of cone angle measurement techniques for the fuel spray from a port fuel injector. Colorado, United States; 2009.

11. Ashgriz N. Handbook of atomization and sprays. New York: Springer; 2011.

12. Zhao F, Lai MC, Harrington DL. Automotive spark-ignited direct-injection gasoline engines. Progress in energy and Combustion Science. 1999;25:437–562.

13. Zhu B, Xu M, Zhang Y, Zhang G. Physical Properties of Gasoline-Alcohol Blends and Their Influences on Spray Characteristics from a Low Pressure DI Injector. Virtual Powertrain Conference. 2010 Oct;

14. Liu H. Science and Engineering of Droplets - Fundamentals and Applications. William Andrew Publishing/Noyes; 2000.

15. Lin SP, Reitz RD. Drop and Spray Formation from a Liquid Jet. Annual Review of Fluid Mechanics. 1998;30:85–105.

16. Deshmukh D, Ravikrishna RV. Experimental studies on high pressure spray structure of biofuels. Atomization and Sprays,. In Press;

17. Guildenbecher DR, López-Rivera C, Sojka PE. Secondary atomization. Exp Fluids. 2009 Jan;46(3):371–402.

18. Apte SV, Gorokhovski M, Moin P. LES of atomizing spray with stochastic modeling of secondary breakup. International journal of multiphase flow. 2003;29(9):1503–22.

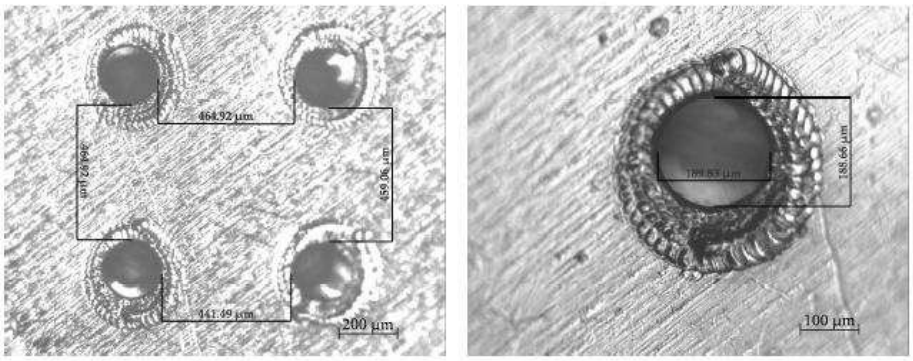

Figure 1: Photograph showing the nozzle face and a closeup image of one orifice. The spacing between orifices marked is ~460 µm, and the orifice diameter is ~190 µm.

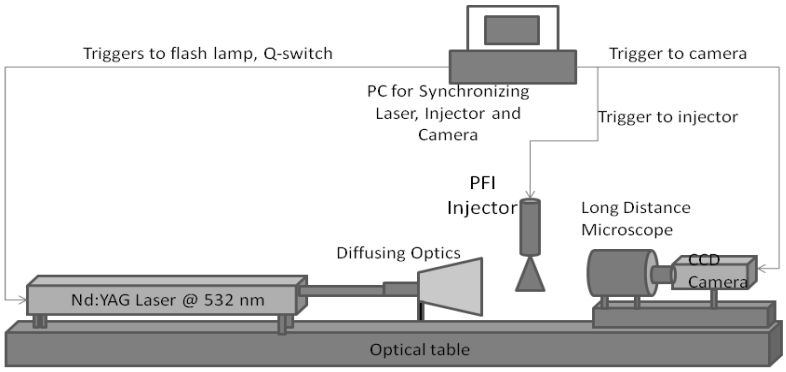

Figure 2: Schematic of the experimental setup

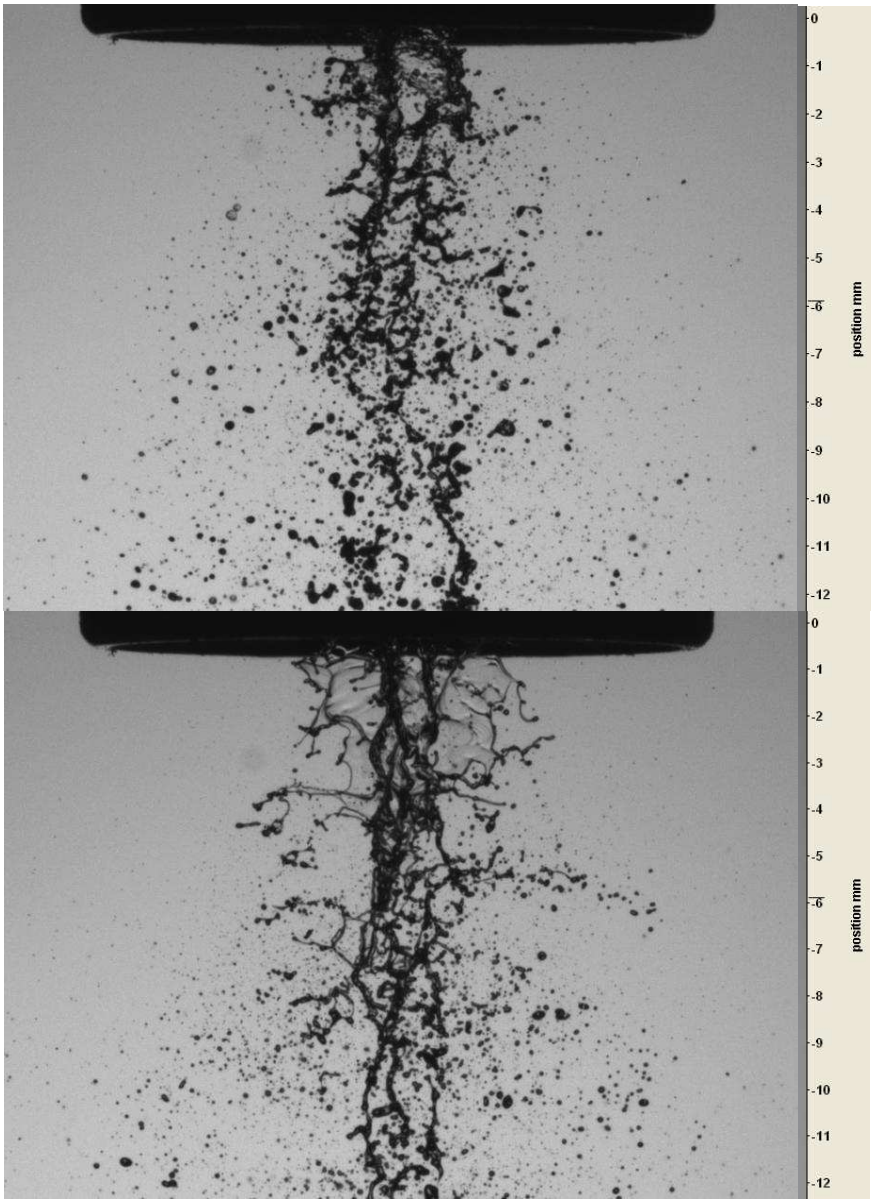

Figure 3: Instantaneous image showing the spray structure of pure gasoline (top), and pure ethanol (bottom) sprays, at an injection pressure of 0.25 MPa

.

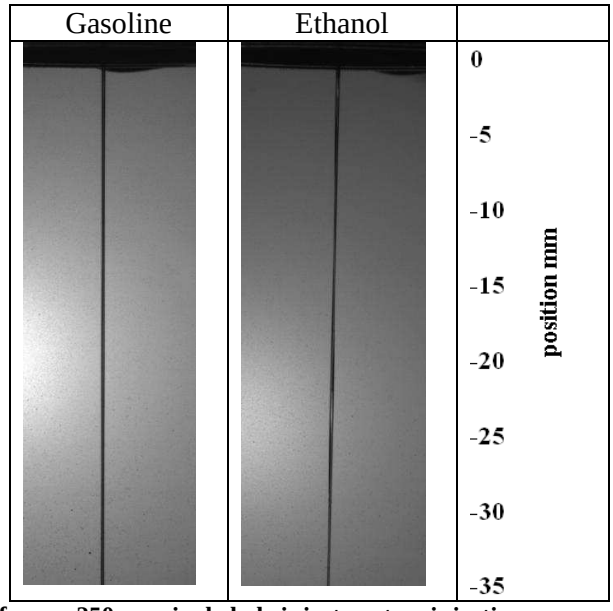

Figure 4: Images from a 250 µm single hole injector at an injection pressure of 0.6 MPa

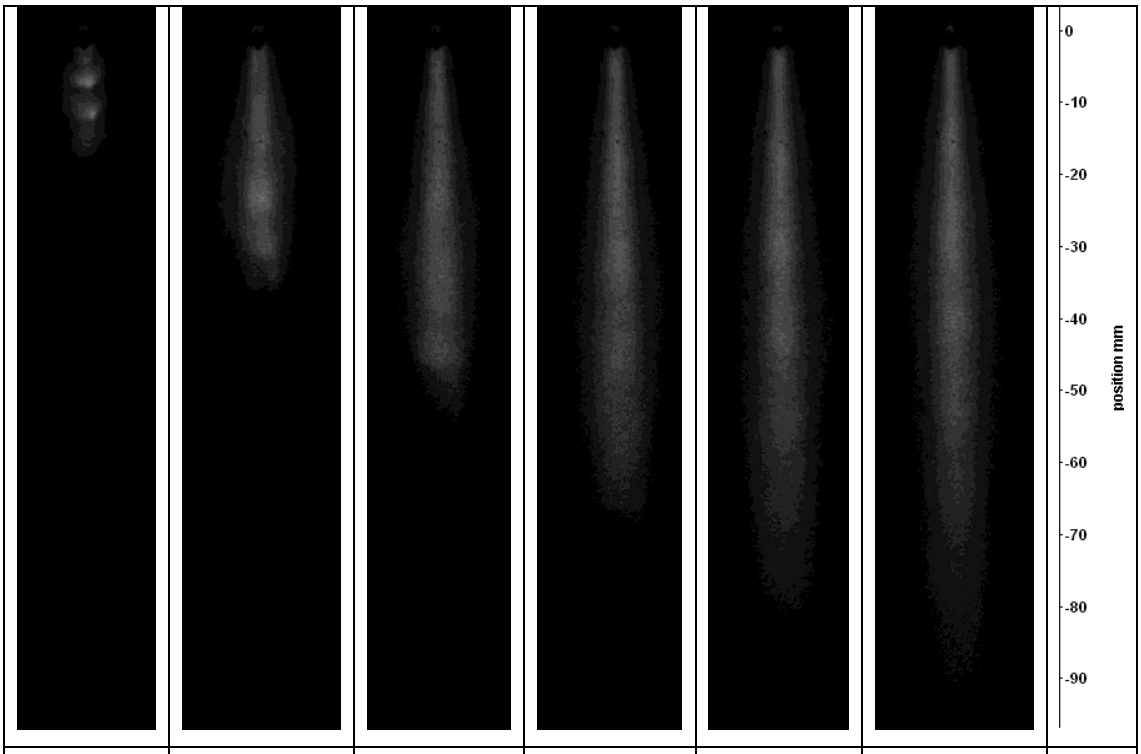

Figure 5: Ensemble averaged images showing the progression of the spray. The time (after the start of the injection pulse) is mentioned below each image.

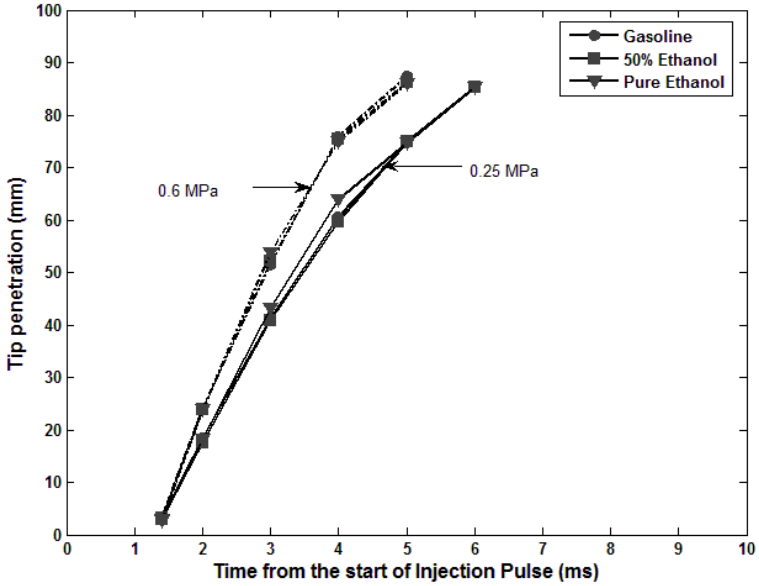

Figure 6: Variation of spray tip penetration with time at injection pressures of 0.6 MPa and 0.25 MPa

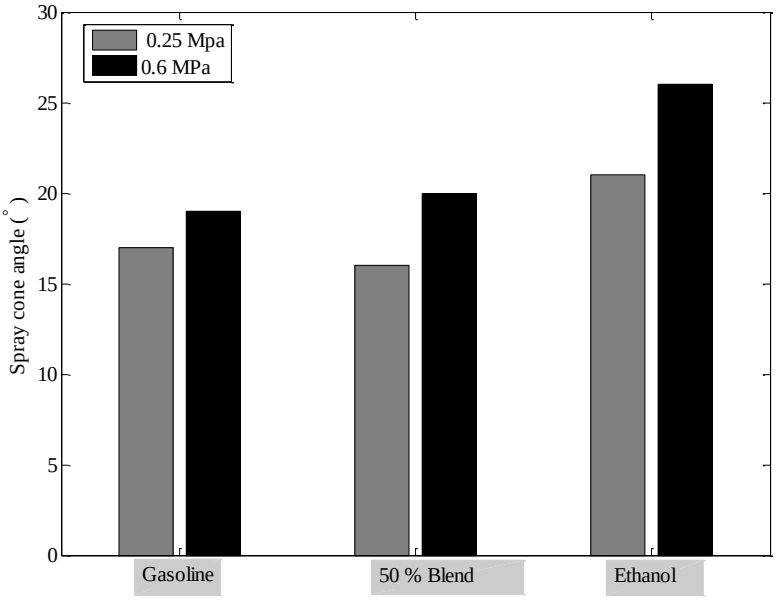

Figure 7: Variation of spray cone angle with pressure for gasoline, ethanol and 50% ethanol blend

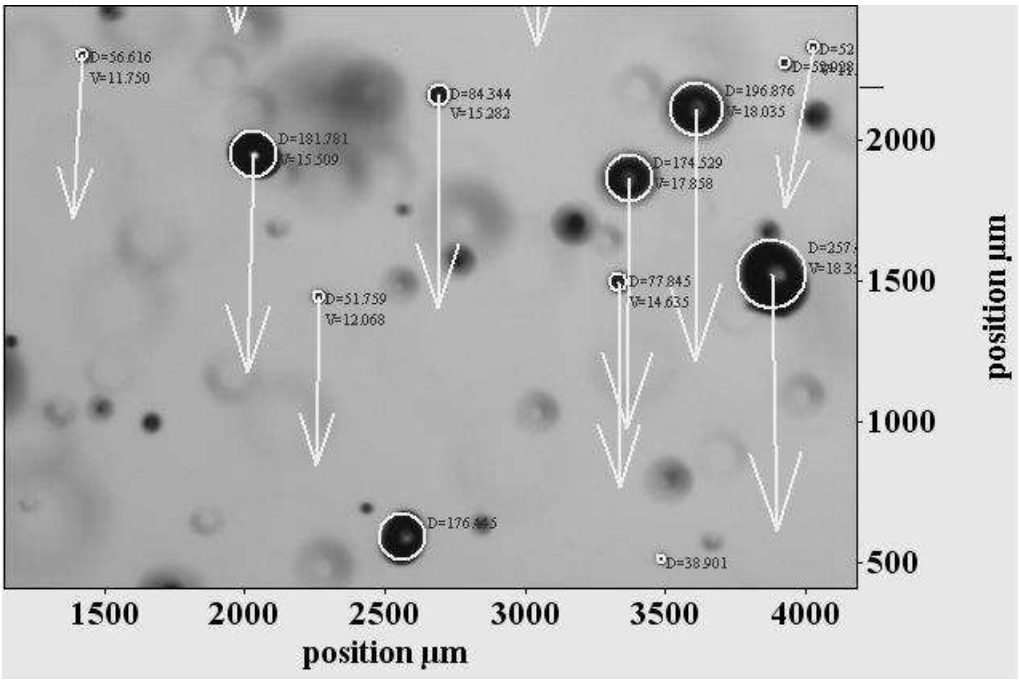

Figure 8: Part of the processed PDIA image showing identified droplets, their diameters and velocities

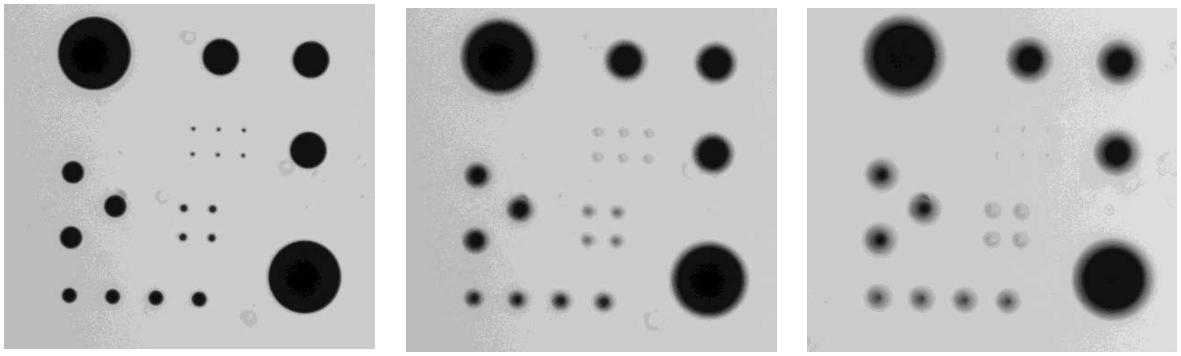

Focused Plane **600 µm away** **1000 µm away**

Figure 9: Images of calibration plate at different distances from the focal plane. The smallest circular dot has a diameter of 10 µm and the largest has a diameter of 200 µm.

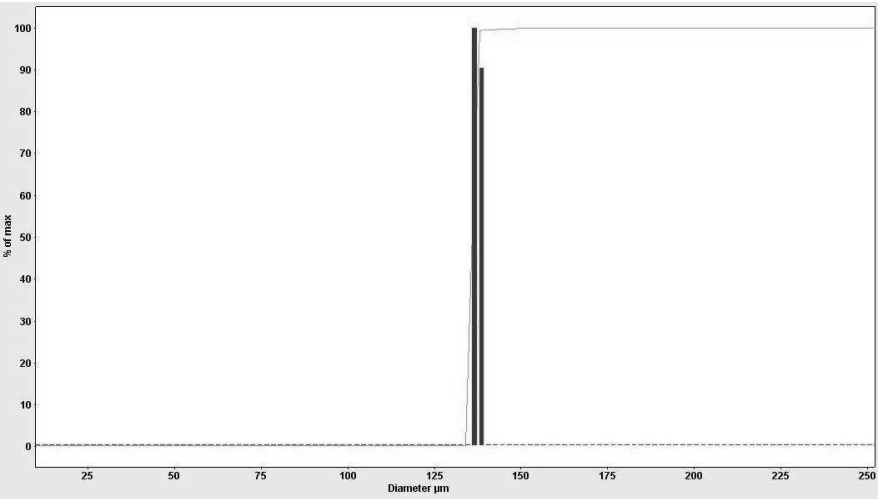

Figure 10: Measured Droplet size distribution for a mono-dispersed droplet stream

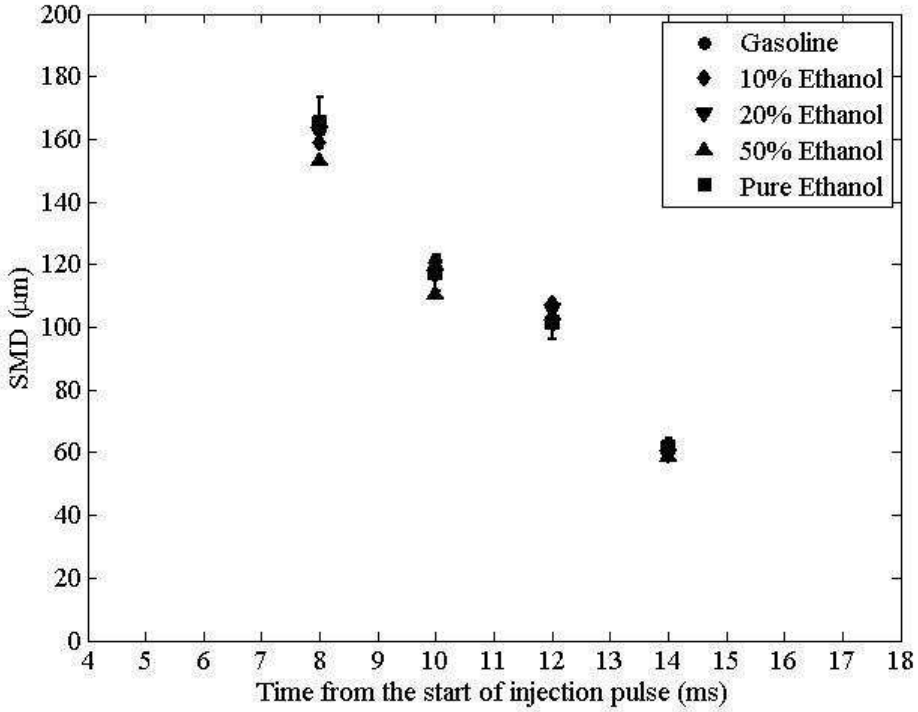

Figure 11: Variation of SMD with time for an injection pressure of 0.25 MPa

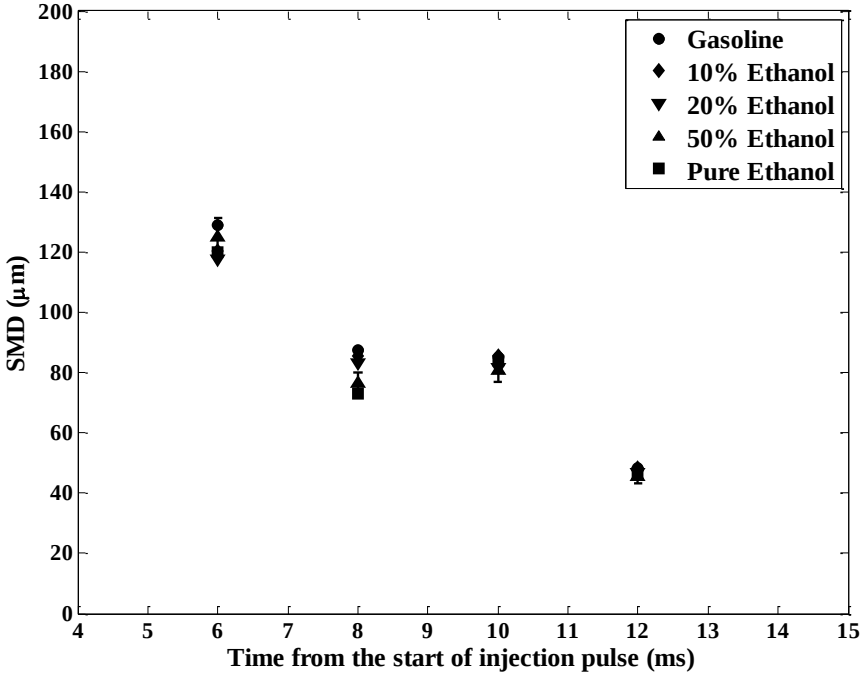

Figure 12: Variation of SMD with time for an injection pressure of 0.6 MPa

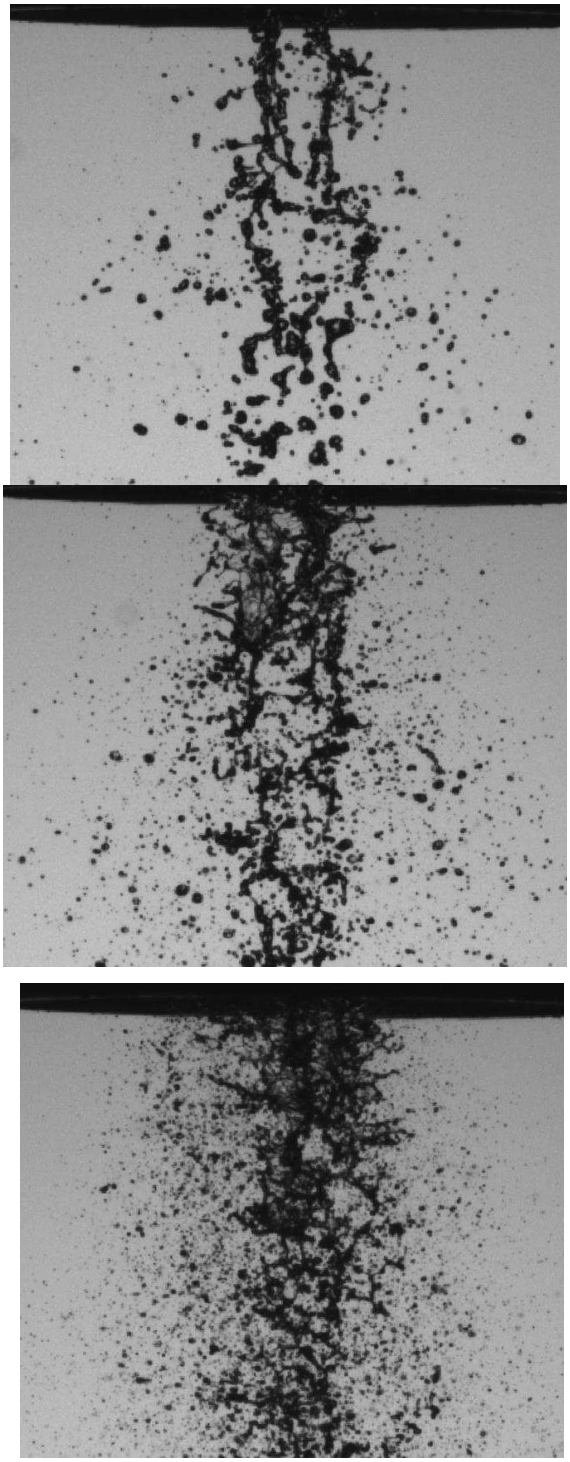

Figure 13: Gasoline sprays at injection pressures of 0.08 MPa, 0.25 MPa, and 0.6 MPa, respectively.

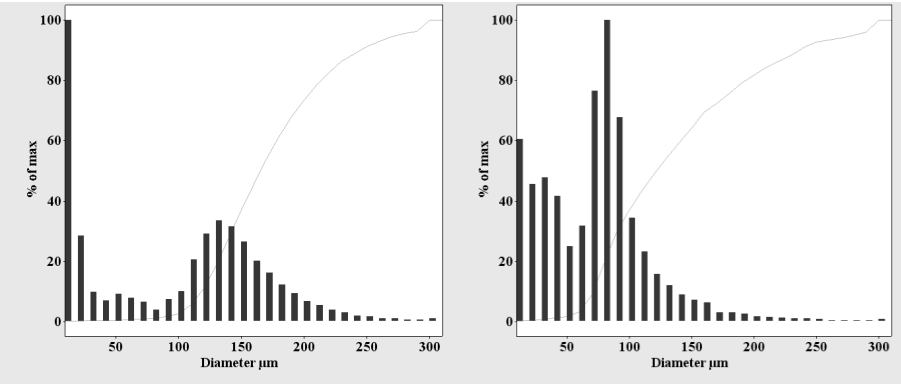

Figure 14: Droplet size distribution for pure ethanol at 0.25 MPa injection pressure, 8 ms and 10 ms after the start of injection, at 100 mm downstream of injector (D10: 95.9 µm and 69.6 µm, respectively)

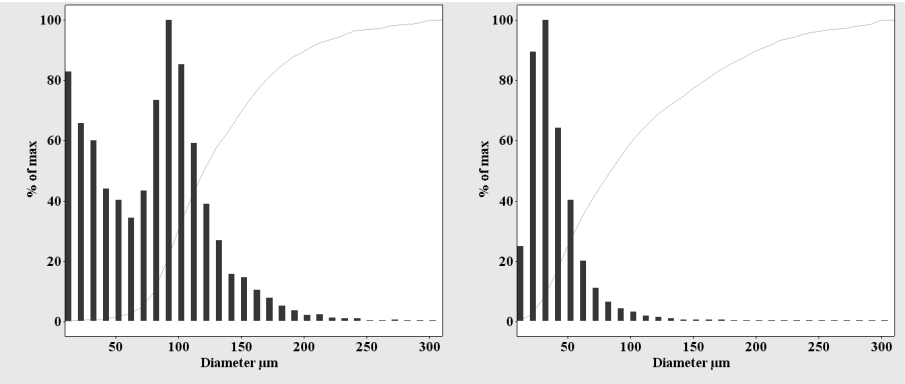

Figure 15: Droplet size distribution for pure ethanol at 0.6 MPa injection pressure, 6 ms & 8 ms after the start of injection, at 100 mm downstream of injector (D10: 75.4 µm and 36.9 µm, respectively)

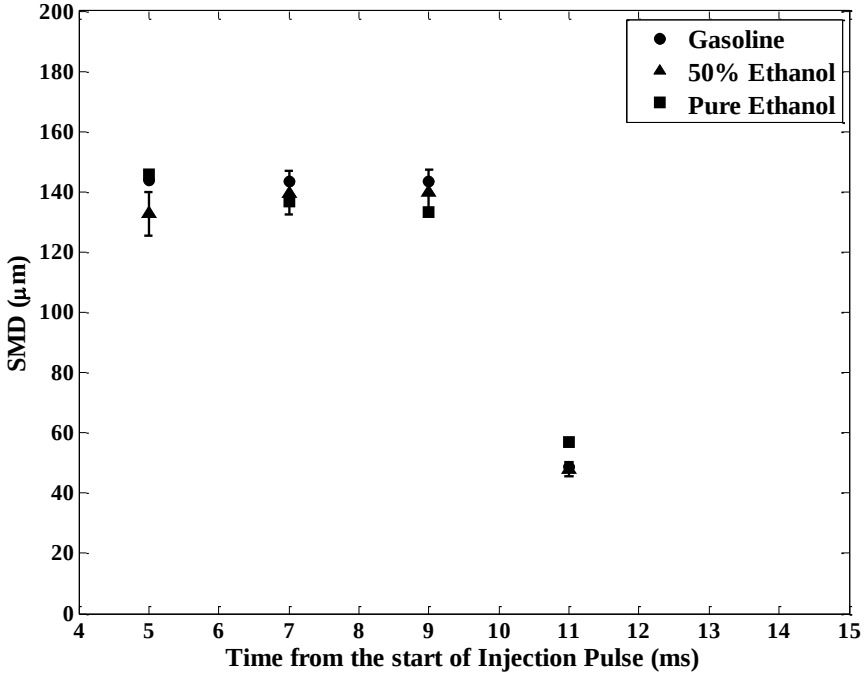

Figure 16: Variation of SMD with time for an injection pressure of 0.25 MPa at 50mm downstream of injector

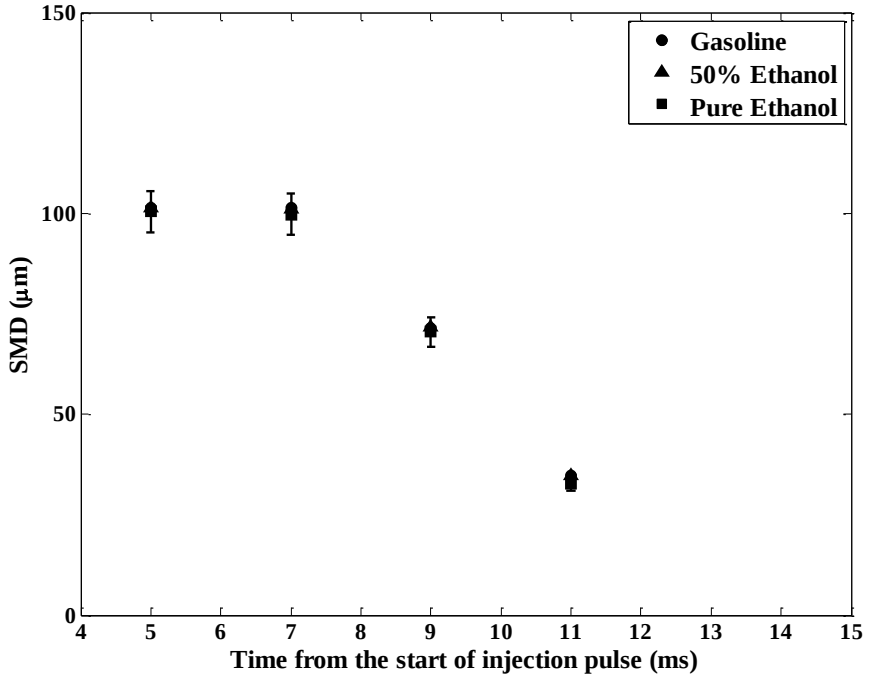

Figure 17: Variation of SMD with time for an injection pressure of 0.6 MPa at 50mm downstream of injector

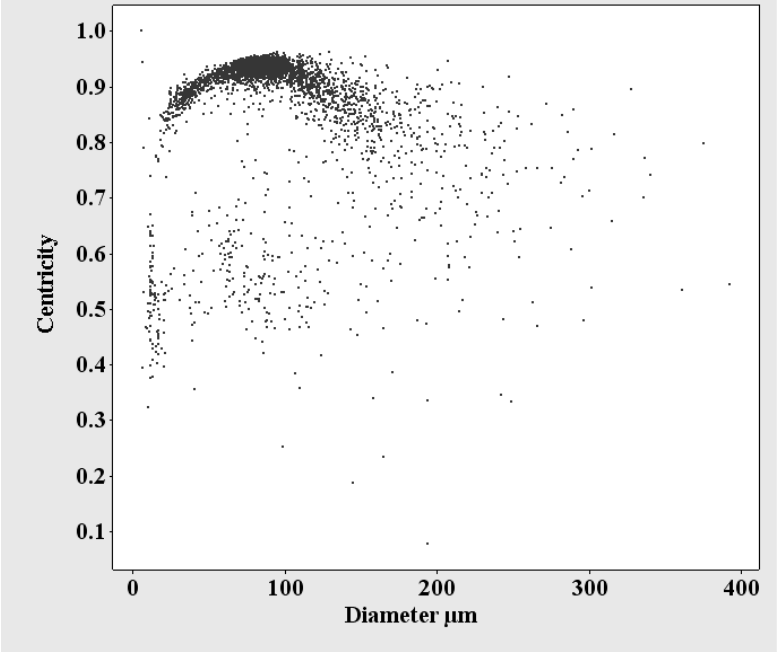

Figure 18: Centricity plot for pure ethanol at 10 ms after SOI for an injection pressure of 0.25 MPa, at a location 100 mm downstream of the injector

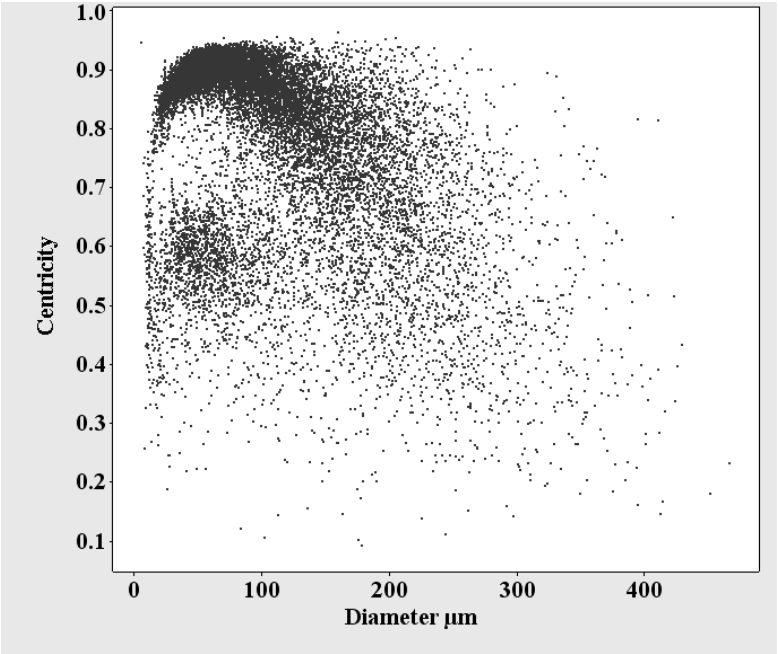

Figure 19: Centricity plot for pure ethanol at 5 ms after SOI at 0.25 MPa, 50mm downstream

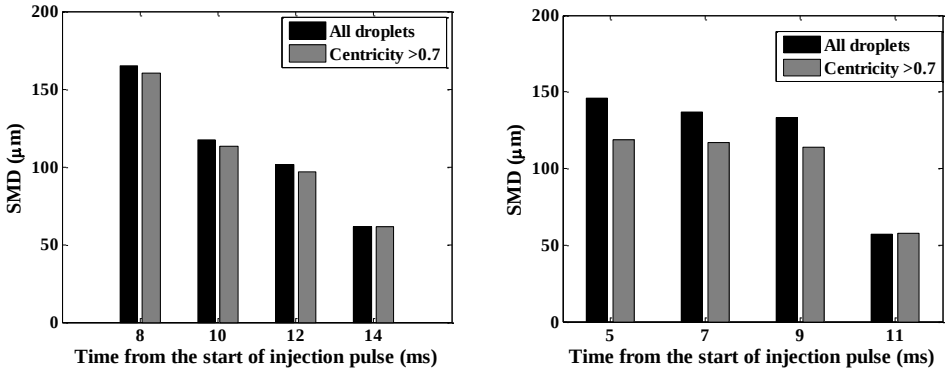

Figure 20: Difference in the SMD values when all droplets, and only droplets with a centricity higher than 0.7 are considered. The results are for a location 100mm downstream (left), and 50mm downstream (right), for pure ethanol spray at an injection pressure of 0.25 MPa

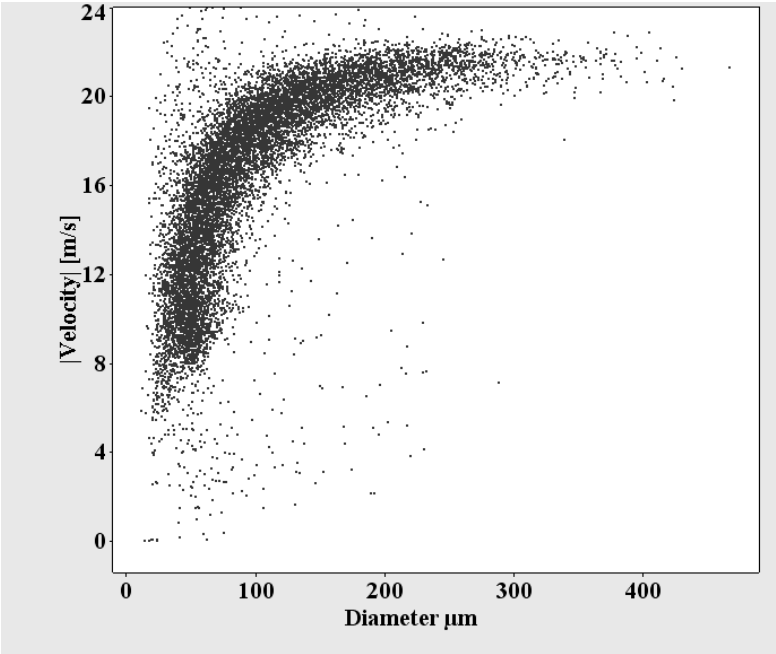

Figure 21: Velocity plot for pure ethanol at 5ms after SOI at 0.25 MPa, 50mm downstream

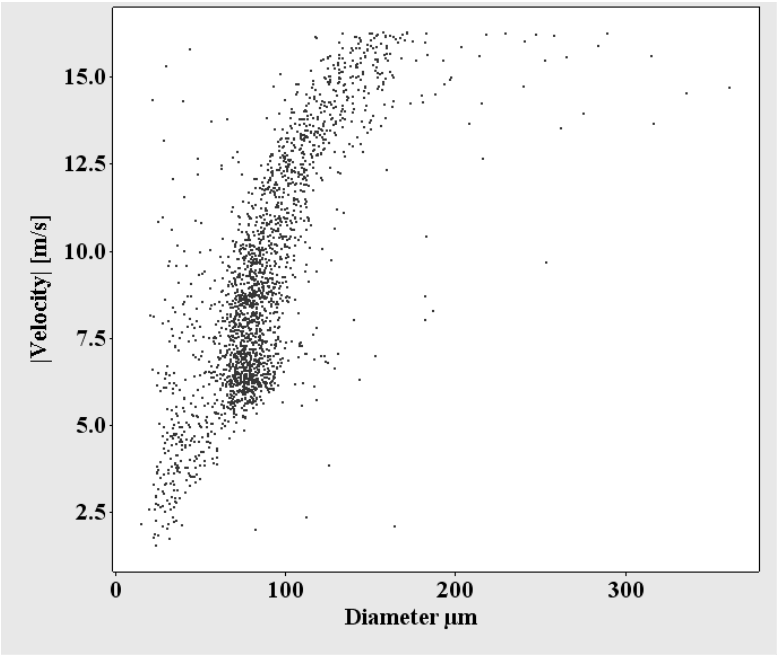

Figure 22: Velocity plot for pure ethanol at 10 ms after SOI for an injection pressure of 0.25 MPa, at a location 100mm downstream of the injector

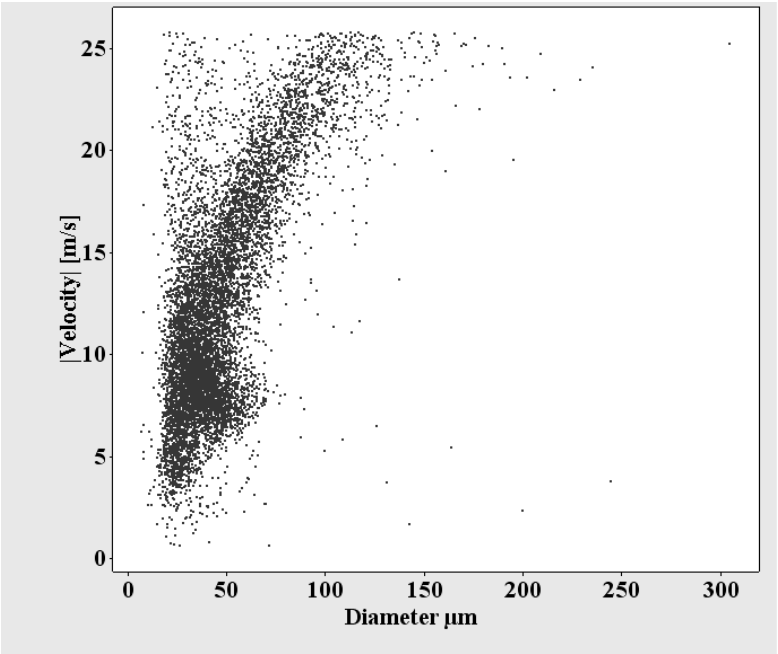

Figure 23: Velocity plot for pure ethanol at 8 ms after SOI for an injection pressure of 0.6 MPa, at a location 100mm downstream of the injector

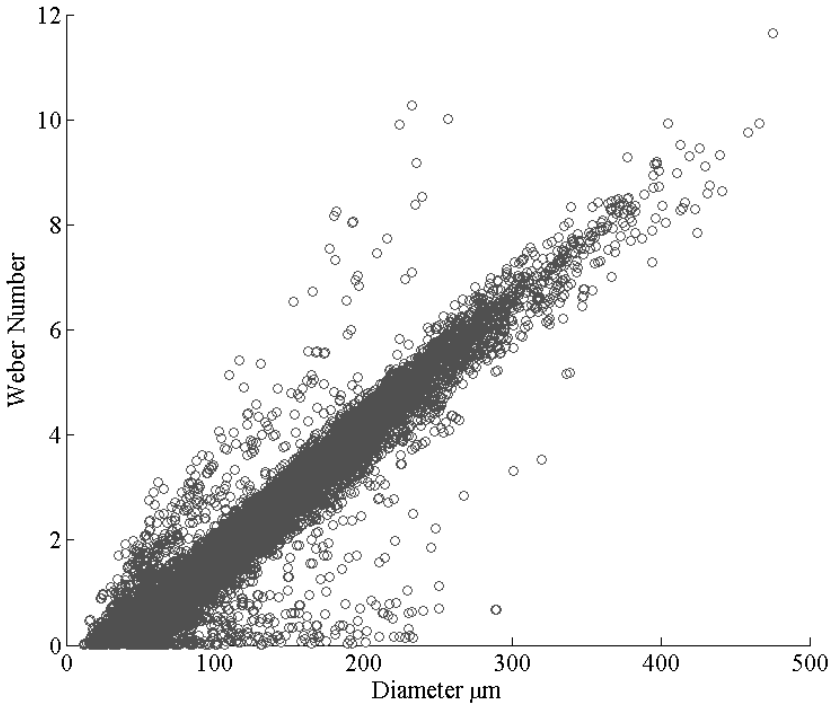

Figure 24: Weber Number of Ethanol Spray at 0.25 MPa injection pressure, at 50 mm axial location and 5 ms after start of injection pulse

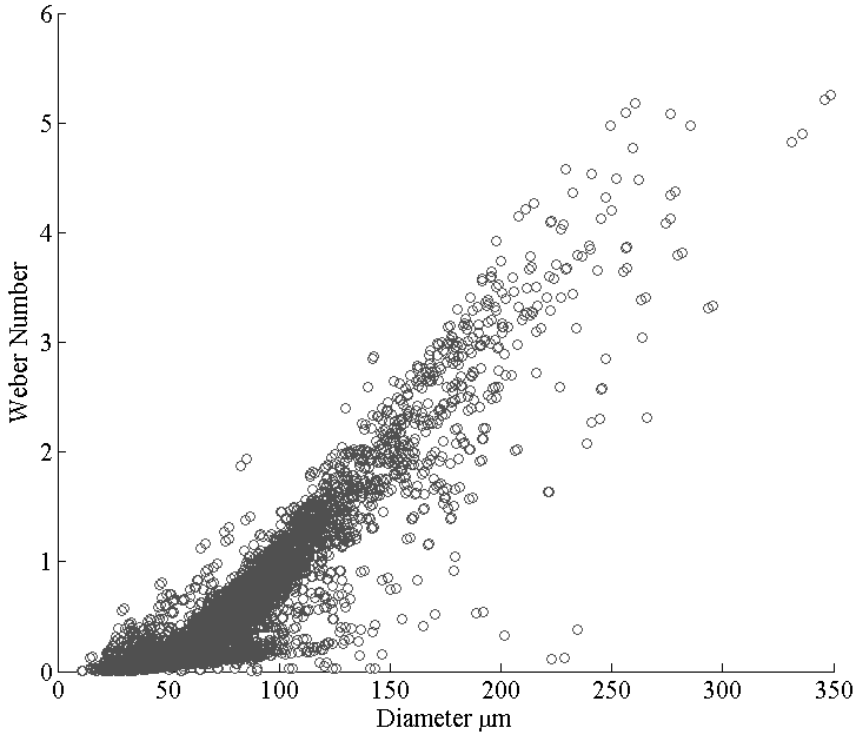

Figure 25: Weber Number of Ethanol Spray at 0.25 MPa injection pressure, at 100 mm axial location and 10 ms after start of injection pulse

Table 1: Mass of fuel injected per pulse (Derived from an average of 200 sprays)

Injection pressure	Gasoline	50% ethanol	Ethanol
2.5 bar	8.75 mg	8.97 mg	9.98 mg
6.0 bar	12.57 mg	12.99 mg	14.39 mg

Table 2: Properties of Gasoline and Ethanol

Property	Gasoline	Ethanol
Density	734 kg/m^3	789 kg/m^3
Viscosity	0.37-0.44 mPa·s	1.19 mPa·s
Surface tension	20.8 mN/m	22.3 mN/m